Anthramycin–DNA Binding Explored by Molecular Simulations

ARTICLE *in* THE JOURNAL OF PHYSICAL CHEMISTRY B · JANUARY 2007

Impact Factor: 3.3 · DOI: 10.1021/jp063155n · Source: PubMed

4 AUTHORS:

Attilio Vittorio Vargiu
Università degli studi di Cagliari
49 PUBLICATIONS **570** CITATIONS
SEE PROFILE

Paolo Ruggerone
Università degli studi di Cagliari
125 PUBLICATIONS **2,071** CITATIONS
SEE PROFILE

Alessandra Magistrato
Scuola Internazionale Superiore di Studi Ava…
77 PUBLICATIONS **1,178** CITATIONS
SEE PROFILE

Paolo Carloni
Forschungszentrum Jülich
320 PUBLICATIONS **6,074** CITATIONS
SEE PROFILE

Anthramycin−DNA Binding Explored by Molecular Simulations

Attilio V. Vargiu,[†,‡] Paolo Ruggerone,*[,‡,§] Alessandra Magistrato,[†,‡] and Paolo Carloni*[,†,‡]

SISSA/ISAS and CNR-INFM-Democritos Modeling Center, Via Beirut 4, I-34014 Trieste, Italy, and CNR-INFM-SLACS and Department of Physics, Università degli Studi di Cagliari, I-09042 Monserrato (CA), Italy

Received: May 23, 2006; In Final Form: August 13, 2006

The anticancer drug anthramycin inhibits replication and transcription processes by covalently binding to DNA. Here, we use molecular simulations to investigate the interaction between this ligand and the dodecanucleotide d[GCCAACGTTGGC]$_2$. We start from the X-ray structure of the adduct anthramycin-d[CCAACGTTG*G]$_2$, in which the drug binds covalently to guanine.[1] We focus on the noncovalent complexes between the oligonucleotide and the anhydro and hydroxy forms of the drug. Molecular dynamics (MD) simulations show that only the hydroxy form lies in front of the reactive center for the whole simulation (∼20 ns), while the anhydro form moves inside the minor groove to the nearest base pair after ∼10 ns. This sliding process is associated to both energetic and structural relaxations of the complex. The accuracy of our computational setup is established by performing MD simulations of the covalent adduct and of a 14-mer complexed with anhydro-anthramycin. The MD simulations are complemented by hybrid Car−Parrinello quantum mechanics/molecular mechanics (QM/MM) simulations. These show that in the noncovalent complexes the electric field due to DNA polarizes the hydroxy and, even more, the anhydro form of the drug as to favor a nucleophilic attack by the alkylating guanine. This suggests that the binding process may be characterized by a multistep pathway, catalyzed by the electric field of DNA.

Introduction

Pyrrol[1,4]benzodiazepine (PBD) cytotoxins[2] exert a powerful antitumoral activity[3,4] by covalently binding to the minor groove of B-DNA. All PBDs share a condensed three-ring moiety featuring a right-handed twist between the phenol and pyrrol rings (rings A and C in Chart 1), which allows them to snugly fit into the backbone of B-DNA. Despite their low molecular weight, PBDs are quite sequence selective, recognizing codes three to seven base pairs (bp's) long.[5,6] Drug binding is believed to proceed by formation of a noncovalent complex (step I):[7]

$$\mathrm{DNA} + \mathrm{PBD} \overset{K_B}{\rightleftharpoons} (\mathrm{DNA{\cdot}PBD})_{\mathrm{noncov}}$$

followed by a covalent linkage (step II):

$$(\mathrm{DNA{\cdot}PBD})_{\mathrm{noncov}} \xrightarrow{k_r} (\mathrm{DNA-PBD})_{\mathrm{cov}}$$

The molecular recognition process is supposed to be driven by (nonspecific) nonbonded interactions and sequence-specific structural features, rather than by specific H-bond patterns.[8] However, the molecular details of this process are not yet fully understood.

A PBD derivative, anthramycin[1] (Chart 1), is one of the very few organic minor groove covalent binders for which the X-ray structure of the covalent complex with an oligonucleotide is available. This drug covalently binds to the exocyclic amino group of guanine through the C11 carbon,[1] showing a modest sequence selectivity for guanines embedded in Pu−G−Pu sequences (namely, AGA-5′ > AGG-5′ ≈ GGA-5′ > GGG-5′).[5−7,9]

The investigation of DNA/PBD complexes may provide useful insights on the factors affecting both reactivity and binding of minor groove covalent binders. In fact, although anthramycin is cardiotoxic,[3,10] a number of its derivatives have shown improved antitumoral activity. In particular, the dimer SJG-136[11,12] is currently in phase I clinical trials in both U.K. and U.S.A. In addition, PBDs have also being used as components of a gene targeting strategy[13,14] aiming at designing molecules able to target a specific cancer-related gene.

Prompted by the biological and pharmacological relevance of PBDs, we have performed molecular dynamics (MD) simulations on both the hydroxy and anhydro putative reactive forms of anthramycin (Chart 1) in complex with DNA. Thanks to the development of both "second generation" force fields[15−17] and accurate methods for handling the long-range electrostatic interactions,[18] in the last years, MD has been successfully used to describe the structural and dynamical properties of nucleic acids[19−22] and their complexes with ligands, providing insights into phenomena not accessible or interpretable by experiments (for a review, see, e.g., ref 23). In this respect, however, we point out that the computational studies on PBDs reported so far have been performed without inclusion of explicit waters and counterions,[10,24−26] which are very important to accurately simulate nucleic acids and their complexes,[19,27,28] as well as their reactivity.[29]

The main aim of our investigation was to obtain insights on step I of the reaction. The drugs were initially positioned in front of the reactive guanine (G*) of d[GCCAACGTTG*GC]d-[GCCAACGTTGGC], based on the X-ray structure of the

* Corresponding authors.
† SISSA/ISAS.
‡ CNR-INFM-Democritos Modeling Center.
§ Università degli Studi di Cagliari.

10.1021/jp063155n CCC: $33.50
Published on Web 11/14/2006

CHART 1

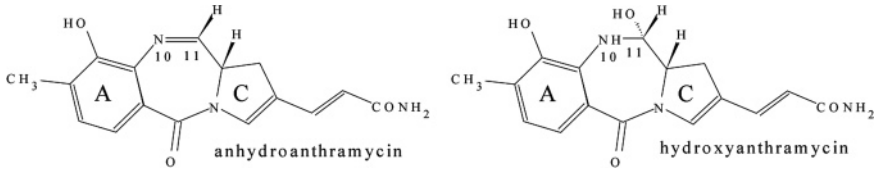

covalent complex.[1] Our simulations show that both forms of the drug, docked in front of the reactive site, induce structural deformations on the DNA frame at its central region, while for the covalent adduct the most significant distortions are seen at the binding region. Interestingly, after 10 ns anhydro-anthramycin slides by one bp step toward the center of the oligonucleotide, where it is stable for the rest of the simulation; this process causes both an energetic and structural relaxation of the complex. Instead, the hydroxy form oscillates around the reactive site for the whole dynamics. Our MD simulations are complemented by a quantum mechanical investigation of environmental effects on the reactivity in the two adducts. By using a hybrid quantum mechanics/molecular mechanics (QM/MM) method,[30] we show that the DNA frame significantly influences the electronic distribution of the reactants; in particular, it appears to polarize the anhydro form of the drug in a way favorable to the alkylation reaction.

Systems and Methods

Classical MD Simulations. The following systems have been investigated in aqueous solution:

Covalent Complex. We built our model (**ANT-DNA** hereafter) starting from the X-ray structure of two anthramycin molecules covalently linked to the oligonucleotide d[CCAACGTTG*G]$_2$.[1] To assess the structural impact of binding, we remove one of the two drugs present in the experimental structure. To limit artifacts associated with terminal effects, we added one CG base pair (bp) at each end.

Noncovalent Complexes. Hydroxy-anthramycin·d[GCCAACGTTG*GC]d[GCCAACGTTGGC] (**ANT·DNA**) and anhydro-anthramycin·d[GCCAACGTTG*GC]d[GCCAACGTTGGC] (**IMI·DNA**) complexes were built: (i) cutting the bond between C11 of the drug and N2 of deoxyguanine, and manually pulling out the drug perpendicularly to the minor groove, until the distance N2−C11 was ∼3.5 Å; (ii) adding the OH group on C11 in the case of **ANT·DNA**, or removing a H atom from N10 in the case of **IMI·DNA** (see Chart 1); (iii) optimizing in vacuo the geometries of the drugs at the B3LYP-6-31G*[31,32] level of calculations with GAUSSIAN.[33]

Reference Systems. (i) **DNA**, which is the 12-mer d[GCCAACGTTGGC]d[GCCAACGTTGGC] in the B conformation, and was constructed with the *nucgen* module of the AMBER package,[34] (ii) hydroxy-anthramycin (**ANT**), and (iii) anhydro-anthramycin (**IMI**). Because we observed a sliding of **IMI** along the oligonucleotide (see Results), we constructed an additional complex between **IMI** and the 14-mer d[CAACGTTG*GCCAAC]d[GTTGGCCAACGTTG] (**IMI·DNAc**). This latter has been built taking **IMI·DNA** as a template (so that the mode of binding of the drug is the same as that in **IMI·DNA**), removing the first two d[GC]d[GC] bp's and adding the d[CAAC]d[GTTG] duplex at the end near the drug. The simulation of **IMI·DNAc** allowed us to check whether such a sliding occurs also when the ligand is located in the central part of the oligonucleotide.

The DNA-containing systems were neutralized by adding sodium counterions. All of the systems were immersed in water boxes, allowing for a solvent shell extending for at least 14 Å around each solute atom (see Supporting Information Table S.1 for detailed information).

The oligonucleotide (except for the nucleoside G* in **ANT-DNA**) was parametrized using the refined Cornell et al. force field,[15−17] while the TIP3P[35] and Aaqvist[36] models were used to represent water and sodium ions, respectively. The structural parameters of the drugs were taken from the gaff[37] database, or constructed with the *parmcal* module of the AMBER package[34] (Table S.2), while RESP[38] charges were obtained using the *resp* utility of AMBER after minimization of the electronic structure with GAUSSIAN[33] (Table S.3). The nucleoside of G* in **ANT-DNA** was parametrized using the same scheme.

Periodic boundary conditions were used, and the electrostatic interactions were calculated with the Particle-Mesh Ewald (PME) method,[18] using a 12 Å cutoff for the real part, as for the van der Waals interactions. NPT simulations at 300 K and 1 atm were performed using the Nosé−Hoover[39,40] thermostat and the Parrinello−Rahman[41] pressure-coupling scheme. A time step of 1.5 fs was set for all of the simulations. H-bond lengths were constrained using the lincs algorithm,[42] and the translational and rotational motions of the center of mass of the solute were removed every 25 MD steps.

Before starting the dynamics, all of the systems underwent geometry optimization in two steps: the first with a harmonic restraint of $k = 150$ kcal/mol imposed to the solute; the second without any restraint. Then, the systems were heated linearly to 300 K in 100 ps of NVT MD (namely, the temperature was increased by 15 K each 5 ps), and as a last step preceding the productive dynamics, 200 ps of NPT runs were carried out. Multi-nanosecond trajectories were finally collected (Table S.1), for a total of ∼140 ns. Although it has been show that the sampling of counterion motion requires very long times,[43] according to recent publications,[21,23,44] the time intervals spanned in our simulations provide good statistics on DNA conformational and helicoidal parameters.

All of the simulations were performed using the GROMACS package.[45,46] The structural parameters of DNA were calculated with the program CURVES 5.2.[47] The minor groove widths were defined as the distances between sugar C4′ atoms, subtracted by two carbon van der Waals radii.[1] A propeller twist and a buckle angle between the pyrrol and the phenol rings of the drug were also defined, according to ref 1. The relative energies of nonbonded interactions were estimated using the terms in the AMBER force field.[16,17,34] The molecular solvent accessible surface area (SASA)[48] of various molecules was calculated with GROMACS,[46] using a probe radius of 1.4 Å. The variation in the hydrophobic SASA, that is proportional to the nonpolar free energy of solvation, was evaluated as $\Delta SASA = SASA_{complex} - SASA_{DNA} - SASA_{drug}$. All contributions to the binding are calculated limitedly to the bp's from G7−C18...G11−C14, directly involved in the binding and covering

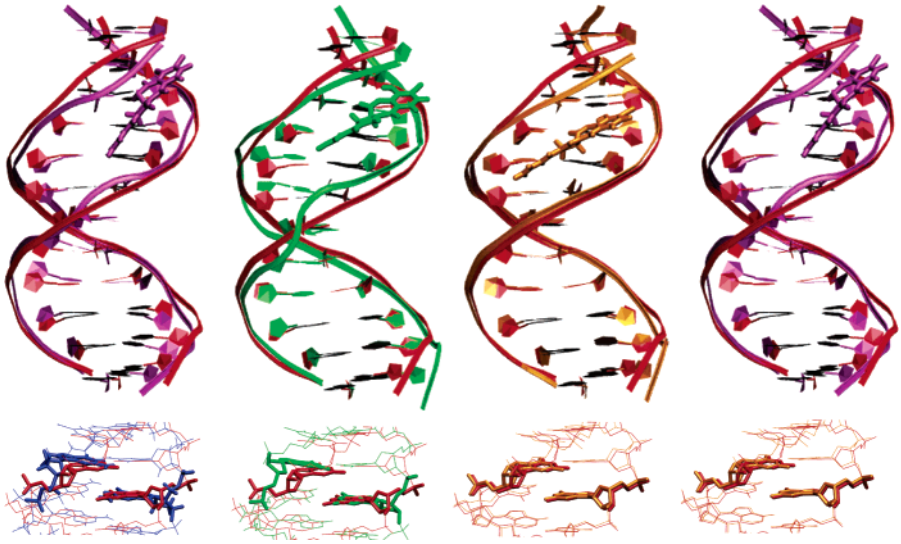

Figure 1. Superimposition between the MD-averaged structure of **DNA** (red) and those of **ANT·DNA** (blue), **IMI·DNA 2** (orange), **IMI·DNA 1** (green), and **ANT-DNA** (magenta). The details show the sugar flips that arise upon noncovalent binding.

the sliding path of anhydro-anthramycin (a test calculation showed that the interaction of the drug with the rest of the oligonucleotide amounts to less than 5% of the total, data not shown).

QM/MM Simulations. The QM/MM scheme allows to investigate at a quantum level the reactive site of the system, taking into account the electrostatic effects of the biomolecular frame, and to dissect between various sources of polarization. In this work, we used the scheme developed by Rothlisberger and co-workers,[30] implemented in the program CPMD.[49] The drug/DNA adducts were partitioned in quantum and classical regions. The first (QM hereafter) comprised the drug and the nucleoside of the reactive guanine G10 (56−59 atoms) and was treated at the density functional theory level[50,51] using the BLYP[31,32] exchange-correlation functional. The guanine was cut at the C1′ carbon, and the valence of this atom was saturated with two capping hydrogens.[52] The remaining part of the system (MM hereafter) was treated using the AMBER[16,17,34] effective potential.

The QM part is contained within a rectangular box of 6000−7000 Å^3 and was treated as an isolated system.[53] Quantum calculations were performed using plane wave decomposition of up to a kinetic energy of 70 Ry, along with pseudopotentials of the Martins−Trouillers type.[54] The electrostatic interactions between QM and MM atoms were calculated using a hierarchical scheme.[30] In this approach, the short-range electrostatic interactions between the QM and MM part were taken explicitly into account within a sphere of radius 5.3 Å around every QM atom using an appropriately modified Coulomb potential that ensures no spill-out of the electronic density. Beyond this first shell and within 10.6 Å, the electrostatic interactions were calculated using the D-RESP charges for the QM atoms. In the outermost region, a multipole expansion scheme was employed. This hierarchical method is fully Hamiltonian and ensures high accuracy in the core region and efficient computation in the region further away from the QM part. The starting structures were taken from the last MD snapshots and then slowly quenched to reach 0 K temperature, to relax the constraints on QM atoms. Subsequently, the systems were slowly heated to 300 K, and NVT simulations were carried out for 3 ps, coupling the systems to a Nosé−Hoover thermostat.[39,40] A time step of 5 au (∼0.12 fs) and a fictitious electronic mass of 600 au were used.

To estimate the amount of polarization within the QM region, Boys orbitals[55] (BOs) were calculated during the QM/MM simulations, and on the basis of their position, we estimated the ionicity of selected bonds. To this aim, following ref 56, we defined a bond ionicity of the A−B bond as $BI_{AB} = (|\vec{d}_A| \cos\theta/|\vec{d}_{AB}|)$, where $\vec{d}_A$ is the position vector of the BO along A−B with respect to A, $\vec{d}_{AB}$ is the position vector of B with respect to A, and θ is the angle between the two position vectors. With this definition, BIs identify electron lone pairs and can be used to visualize the polarization of selected bonds. For example, a value of BI_{AB} much lower than 0.5 indicates a strong polarization of the electronic charge toward A.

Results and Discussion

MD Simulations. In this section we discuss results from classical MD simulations, focusing in particular on the noncovalent complexes.

Covalent Complex. We summarize here our results from a 20 ns long MD simulation of the **ANT-DNA** covalent complex in aqueous solution, and compare its features with those of the X-ray structure[1] in order to validate our computational setup. The average root mean square deviation (rmsd) between the average structure of the 10-mer d[CCAACGTTG*G]d-[CCAACGTTGG] and the X-ray structure is 3.3 Å. Its average rmsd with respect to **DNA** (calculated without the drug) is 1.6 Å: consistently, binding by the drug does not induce any appreciable bending of the DNA axis (Figure 1), in agreement with experimental findings.[1] The structural determinants (Figures 2 and 3) and the B-factors of the complex agree well with the experimental ones, except around the region C24−G1...T20−A5, from where we removed a second drug bonded to G22 in the X-ray structure (see Methods). It turns out that the bonding by the drug affects the DNA frame essentially in the binding region.

The H-bond pattern between the drug and the oligonucleotide however differs significantly with respect to the experiment. In MD simulation, one to four *direct* H-bonds are formed and broken during the dynamics (average number 1.7), involving mostly the OH_{Ant} group, that interacts with both NH_{G11} and O_{C15}, and the acrylamid tail of the drug (Figure 4 and Table S.4). In addition, one to three water-mediated H-bonds are established

TABLE 1: Comparison between X-ray and Calculated Acceptor−Donor Distances Involving Drug and DNA

	$N3_{G11}...O9_{An}$ (Å)	$O2_{C15}...O9_{An}$ (Å)	$O2_{C15}..N10_{An}$ (Å)	$N3_{G11}...N10_{An}$ (Å)	$O2_{T9}...N15_{An}$ (Å)	$O4'_{G10}...N15_{An}$ (Å)
X-ray	3.9	3.1	3.4	3.7	2.9	3.3
MD	4.0 ± 0.3	2.9 ± 0.3	2.9 ± 0.2	3.3 ± 0.2	5.3 ± 0.4	4.9 ± 0.9

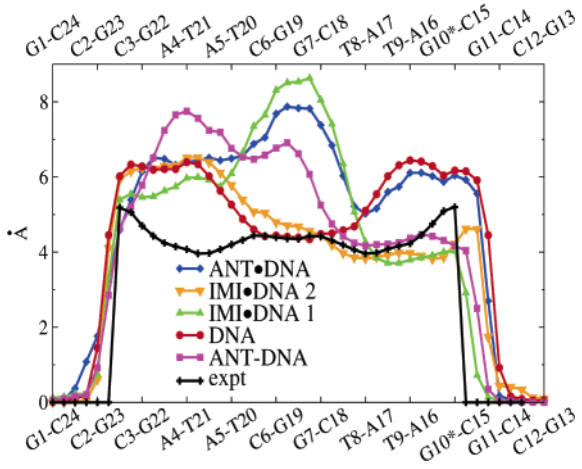

Figure 2. Average values of the minor groove width of **DNA** (red), **ANT·DNA** (blue), **IMI·DNA 1** (green), **IMI·DNA 2** (orange), and **ANT-DNA** (magenta), calculated between C4′ sugars.

between $HN15_{Ant}$ and $O2_{T9}$, $O4'_{G10}$, and $N3_{A17}$. These waters push the drug tail toward the strand containing A17. As a consequence, $HN15_{Ant}$ links to N_{A17} and loses the contact with $O2_{T9}$ and $O4'_{G10}$. Note that these bridging waters are not present in the X-ray structure. Three *direct* H-bonds are also present in the X-ray structure, that exhibits totally six H-bonds (Table 1). This discrepancy might be due to the effect of packing forces in the crystallographic structure, which are particularly important at the ends of the oligonucleotide.[8] According to our results, the H-bond pattern connecting the drug and the DNA has a minor role in stabilization, as compared to ref 1. However, the aqueous solvent, not detected by the X-ray experiment, might assist significantly the formation of water-mediated H-bonds.

We conclude that the MD structure of **ANT-DNA** reproduces most of the experimental data, apart from the drug−DNA H-bond pattern, which may differ from the X-ray one mostly because of environmental effects.

Noncovalent Complexes. In this section, we provide insights on aspects of the molecular recognition process between anthramycin and DNA, through MD simulations of the noncovalent complexes **IMI·DNA** and **ANT·DNA**, and we compare them with the isolated reactants in water solution (**ANT**, **IMI**, and **DNA**), as well as that of the covalent adduct **ANT-DNA**, discussed above.

Structural Analysis and Sliding of Anhydro-Anthramycin. The structural stability of the systems has first been analyzed in terms of deviations from their averages, as well as from those of canonical B-DNA and A-DNA. Figure 5 shows that the rmsd of the oligonucleotides assumes two different values for several nanoseconds in the noncovalent complexes, while it is almost constant in **DNA** and **ANT-DNA**. Consistently, while for **DNA** and **ANT-DNA** the rmsd is 4 Å with respect to B-DNA and 5 Å with respect to A-DNA for the whole simulation, the noncovalent complexes assume for several nanoseconds conformations having lower rmsd relative to A-DNA than to B-DNA.

The most interesting event observed is a sliding of the drug in IMI·DNA along the minor groove, toward the central part of the oligonucleotide (from site **1**, configuration **IMI·DNA 1,** to **2**, configuration **IMI·DNA 2**, in Figure 6), which occurs after 10 ns. Interestingly, shuffling and translocation have been observed experimentally for other DNA-binding drugs.[57,58] The drug moves by one base pair rm (bp) step, so that $C11_{Ant}$ is located in the vicinity of T9 in **IMI·DNA 2**, and keeps the new position for the rest of the simulation. In contrast, in **ANT·DNA**, the drug is stable around its binding site for the entire dynamics (20 ns). It is interesting to test whether **ANT** would move back if initially located in the "slipped" position of **IMI**. To this aim, we performed MD simulations in which **ANT** is docked in the nonreactive site (with the reactive carbon between bases T8 and T9). Two slightly different configurations were chosen. Both MD simulations, carried out for 2.5 ns, show that the drug does not move back to the reactive site: in one, the average distance between $C11_{ANT}$ and $N2_{G10}$ passes from 6.3 to 5.6 ± 0.3 Å (average value over the last 2 ns); in the other, from 7.4 to 7.6 ± 0.3 Å. These results suggest that movements of **ANT** from one "site" to another most probably are not kinetically driven.

A key issue to be addressed is on whether the sliding process is due (totally or in part) to the choice of the model, that is, by having positioned the drug near the end of the oligonucleotide rather than in its center. In fact, nucleobases and ligands in such positions might be subjected to different electrostatic and dynamical stresses. To quantify the relevance of end effects on the properties of the biomolecular frame, we have compared features of **DNA**, that is, the oligonucleotide in aqueous solution, in its central ($d[ACGT]_2$) and terminal ($d[TGGC]_2$) parts. The rmsd's with respect to the average structure turn out to be very similar (1.4 ± 0.3 Å vs 1.3 ± 0.3 Å), and the flexibilities, measured as rmsf's, are identical (0.9 ± 0.3 Å). The differences in electrostatic forces acting on the base atoms are very small, within 15% (Figure S.1). Furthermore, we have constructed two

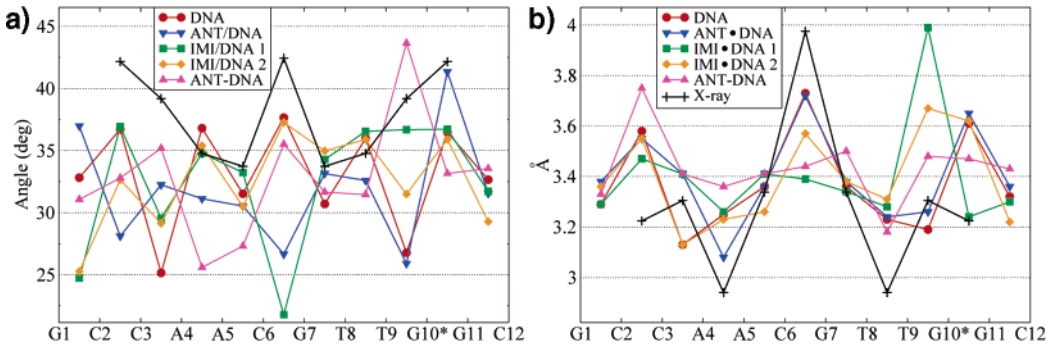

Figure 3. Average values of selected helical parameters (a, twist; b, rise) of **DNA** (red), **ANT·DNA** (blue), **IMI·DNA 1** (green), **IMI·DNA 2** (orange), and **ANT-DNA** (magenta).

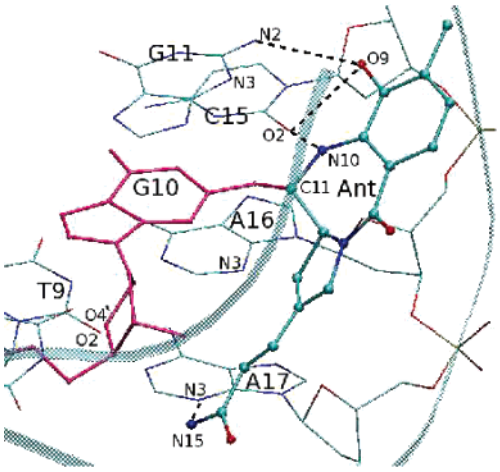

Figure 4. Drug/oligonucleotide H-bonds in **ANT-DNA** (MD structure).

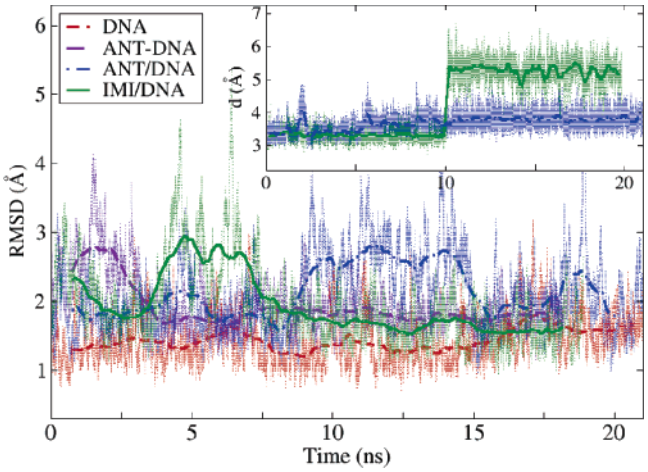

Figure 5. Mass weighted rmsd's of the oligonucleotides in **ANT·DNA**, **IMI·DNA**, **ANT-DNA**, and **DNA**, calculated for heavy atoms after least-squares (LSQ) fit to the average structures in solvent. Running averages are reported as bold lines. The inset reports the distance between reactive atoms $N2_{G11}$ and $C11_{Ant}$ in the noncovalent complexes.

more models other than **IMI·DNA**. In the first, the system is the same, but the initial conditions (in particular the docking of the drug, done manually) are different; a 20 ns MD simulation of the model in aqueous solution shows that a sliding of the drug occurs after 10 ns (note that this is quite a long time in MD simulations with explicit solvent and counterions[20,23,28,44]). In the second, which also has been simulated for 20 ns, **IMI** is docked in the center of the 14-mer d[CAACGTTG*GCCAAC]d-[GTTGGCCAACGTTG] (**IMI·DNAc**). In this case, the same sliding process occurs after 15 ns; in addition, the flexibility, minor groove width, and electrostatic field acting on the drug turn out to be very similar to those of **IMI·DNA** (Tables S.5, Figures S.2 and S.3).

On the basis of results from the structural analysis of **DNA** and from three independent simulations, we suggest that the sliding of the drug is caused by a stabilization of the drug in a position other than the "reactive" one, and we proceed to a structural and energetic analysis of the process.

Structurally, the sliding of the drug is accompanied by a significant rearrangement of the DNA frame (mirrored by a decrease of 8 kcal/mol of the internal energy): in fact, the average structure of the complex before the sliding (**IMI·DNA 1**) shows large deformations with respect to those of **DNA** and **ANT-DNA**, in particular at the central region (Figure 1). The plot of the average minor groove widths (Figure 2) shows the

Figure 6. Superimposition of the **IMI·DNA** MD-averaged structures before (green, **1**) and after (orange, **2**) 10 ns. The drug moves by 1 bp steps. The mean distances between reactive atoms $N2_{G11}$ and $C11_{Ant}$ are respectively 3.3 ± 0.2 Å in **1** and 5.6 ± 0.5 Å in **2**. This and the other images shown in the paper are produced with the programs VMD[75] and gOpenMol.[76,77]

presence of a large unwinding in this region relative to **DNA** and **ANT-DNA**, which is correlated to a flip of the χ glycosidic dihedral at G7 and G19 from anti (−120°) to high anti configuration (−70°, Figure 1). The same findings come out from the analysis of helicoidal inter-base-pair parameters (Figure 3). The oligonucleotide after the sliding (**IMI·DNA 2**) becomes structurally similar to **DNA** (Figures 1 and 3), and the minor groove narrows, in particular in the central region of the oligonucleotide (Figures 1 and 2).

The other noncovalent complex (**ANT·DNA**) assumes also a conformation differing from those of **DNA** and **ANT-DNA** particularly in its middle (Figures 1−3). However, the minor groove has almost the same width as that in **DNA**, due to the presence of the OH11 group of **ANT** (Chart 1). Summarizing, both noncovalent complexes with the drug positioned in front of the reactive site exhibit significant rearrangements in the center of the oligonucleotide with respect to **DNA** and **ANT-DNA**. Upon sliding of **IMI**, the conformational parameters recover values close to those of **DNA**.

Some values of the helical parameters in Figure 3, like high twist and rise and negative roll, are typical of the BII-DNA backbone conformation.[59] BI/BII equilibria can be influenced by ligands, to optimize contacts between partners and to allow the formation of water-mediated H-bonds.[60,61] In fact, we find that the binding of the drug affects these equilibria (data not shown), even if a correlation between binding and conformational changes of the backbone is not easy to rationalize. For example, binding either imposes freezing of certain parameters or allows a major variability of others. In addition, the presence of a low twist (and rise) at CG steps (like in C_6G_7) in MD simulations has been recently correlated to unusual α/γ backbones at the adjacent 5′ step.[44] We found indeed along the backbone some flips of α/γ to stable states other than the canonical g^-/g^+, but they appear to not be correlated with the low twist at C_6G_7. The lifetimes of these conformations are supposed to be larger than typical MD time scales,[43] yet our and other simulations do observe them,[44] even if in almost all the cases reverse transitions are absent. The origin of their appearance has not been elucidated yet, although it might be related to the force field parametrization.

Also, the drugs exhibit a slight distortion upon binding, as shown by the average values of the propeller and twist angles

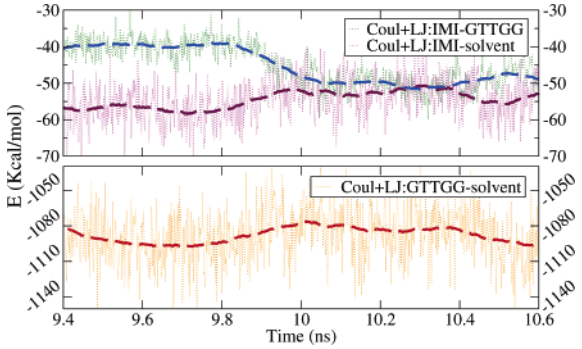

Figure 7. Variations of the nonbonded (electrostatic + LJ) energy of the drug−d($G_7T_8T_9G_{10}G_{11}$)d($C_{18}A_{17}A_{16}C_{15}C_{14}$), drug−solvent, and solvent−d($G_7T_8T_9G_{10}G_{11}$)d($C_{18}A_{17}A_{16}C_{15}C_{14}$) moieties, upon sliding of anhydro-anthramycin (dashed lines correspond to running averages performed on blocks of 100 steps). The sliding process is associated with an increase of ~10 kcal/mol in the interaction energy between the drug and the dodecamer.

TABLE 2: Propeller Twist and Buckle of the Drugs (In Parenthesis Are Reported Available Experimental Results; Data Labeled with an Asterisk Refer to the O11−Methyl Ether of the Drug)

Angle (deg)	ANT-DNA	ANT·DNA	ANT	IMI·DNA 2 IMI·DNA 1	IMI
Propeller	31 ± 5 7 (37.1)	26 ± 8	22 ± 8 (34.4*)	22 ± 7 29 ± 7	26 ± 9
Buckle	13 ± 6 (17.6)	10 ± 5	12 ± 6 (8.2*)	8 ± 4 8 ± 4	9 ± 5

TABLE 3: LJ and Coulomb Interaction Energies Extracted from the Nonbonded Terms of the AMBER Force Field[16,17]

Interaction (kcal/mol)	ANT·DNA	IMI·DNA 2 IMI·DNA 1	ANT-DNA
LJ	−30 ± 2	−40 ± 3 −33 ± 3	−34 ± 3
Coulomb	−12 ± 3	−11 ± 3 −8 ± 3	−20 ± 4

reported in Table 2. Despite the high standard deviations, twist seems to be anti-correlated with the degree of binding, with the only exception of **IMI·DNA 2**. The buckle instead does not change significantly upon binding.

The energetic analysis has been performed using the nonbonded terms of the AMBER force field[15−17] for an approximate estimate of the interaction energies. Although the number of drug−DNA H-bonds is reduced in going from **1** to **2** (two vs three in Table S.4), the overall interaction energy increases by few kcal/mol (Figure 7). This mirrors a better accommodation of the drug into the DNA minor groove after the sliding, increasing the hydrophobic contact area by 4% (Table 4). As a result, the twist of the drug decreases (29 vs 22° in Table 2), allowing a better delocalization of π orbitals on the drug. The entropy change associated with the sliding process turns out to be very small, as: (i) the first shell of waters surrounding the drug and the binding site does not change, as shown by a calculation of the radial distribution function of waters around the binding region (data not shown); (ii) the conformational entropy of the DNA (calculated with the Schlitter's formula[62]) is unchanged.

Within the limitations of these simple estimations, we conclude that the sliding of the drug is mainly due to a gain in nonspecific interactions with the DNA frame, accompanied by a release of the structural stress accumulated by this latter under the presence of the drug.

Other Features of **IMI·DNA 2** and **ANT·DNA**. The LJ interactions account for ~70−80% of the nonbonded energy for both systems, while electrostatics plays a minor role (Table 3). Note that the LJ (Coulomb) interaction is slightly stronger (weaker) in **IMI·DNA 2** than in **ANT·DNA**, possibly because of the presence in the latter of the OH11 group, that prevents the drug from being very close to the DNA backbone. Consistently, the relative decrease of the hydrophobic SASA[48] upon formation of the complex is larger in **IMI·DNA 2** than in **ANT·DNA** (Table 4), corresponding to a larger relative gain in the nonpolar contribution to the free energy of solvation. Thus, **IMI** establishes a more favorable nonbonded interaction with the DNA frame with respect to **ANT**. In the covalent complex, the electrostatic energies become comparable to the LJ ones (Table 3): in fact, the formation of the covalent bond shortens the distances between charged groups, inducing a different distribution of the electronic density on the reactants (see Table S.2).

Interestingly, the H-bonds between the solvent and **IMI**, **ANT**, and **DNA** (calculated only for the atoms at the drug−DNA interface) are only partially replaced in the noncovalent complexes (Table 5). Specifically, drug−DNA H-bonds are formed between G10, G11, and A16 nitrogens, $O4'_{G11}$, and O9, O11, and N10 on the drug (see Figure 4 and Table 5). No water molecules are present between the reactive guanine G10 and the drugs, as should be expected for extended aromatic systems making favorable hydrophobic interactions with the DNA backbone. However, the presence of the OH11 group in **ANT·DNA** allows the entrance of water(s) in the region between the drug and the DNA backbone (Table 5).

On the basis of these results, we suggest that the formation of the complexes has an important entropic contribution, and their stabilization, even in a highly charged system like the minor groove of DNA, is mainly due to hydrophobic contacts.

Reactant Polarization. DNA is a polyelectrolyte, and it may produce large electric fields on the reactants. We investigate the electrostatic effect of the biomolecular frame on the electronic structure of the reactants (the drug and its guanosine target) by 3 ps QM/MM simulations on **ANT·DNA** and **IMI·DNA 1**. Within this scheme, the drug and the reactive guanosine are treated at a quantum level, while the rest of the system is parametrized using the AMBER[16,17,34] effective potential. Thus, the QM/MM scheme allows one to dissect the source of polarization into various contributions, namely, those due to the DNA and the solvent, by switching off their charges. We also assess the amount of reciprocal polarization of the reactants by performing additional QM calculations in vacuo.

Our QM/MM simulations suggest that the biomolecular frame alters significantly the electric field of the reactants, in particular the region between the reactive atoms $N2_{G10}$ and $C11_{drug}$ (Figure 8). The polarizing field created by the environment turns out to be due almost completely to the DNA frame, since identical results are obtained in calculations in which the charges of the solvent are switched off (data not shown). The DNA field is directed from $N2_{G10}$ to $C11_{drug}$ in **IMI·DNA 1**. Thus, this field may assist the alkylation reaction by rendering $C11_{drug}$ more electrophilic, that is, creating electrostatic conditions very favorable for a nucleophilic attack. Instead, in **ANT·DNA**, the largest effect occurs in proximity of the amino group of G10. Thus, in this latter case, the DNA field is expected to enhance the reactivity neither of the drug nor of the DNA. These results are in agreement with experimental findings,[63,64] indicating the anhydro form as the most reactive.

A measure of the polarity of chemical bonds is given by bond ionicity indexes (BIs). For the bond between atoms A and B, a BI of <0.5 (>0.5) indicates a shift of the center of mass of the

TABLE 4: Calculated Hydrophobic SASAs (The Hydrophobic Effect Plays a Role in the Formation of the Complex: A Negative Value of ΔSASA upon Solvation in Water Corresponds to a Gain in the Nonpolar Part of the Solvation Free Energy)

	IMI	ANT	GTTGG	IMI·CTTGG	ANT·GTTGG	ANT-GTTGG
SASA (Å)	191 ± 5	161 ± 5	764 ± 17	667 ± 18 (**2**) 709 ± 17 (**1**)	746 ± 25	739 ± 21
ΔSASA (Å)				−288 (30%, **2**) −246 (26%, **1**)	−179 (19%)	−216 (26%, IMI) −186 (20%, ANT)

TABLE 5: Total Number of Persistent H-Bonds (Present For More Than 10% of the Simulation Time) Formed by the Drug and the Five bp's $d(G_7T_8T_9G_{10}G_{11})d(C_{18}A_{17}A_{16}C_{15}C_{14})$ Involved in The Binding (Averages and Standard Deviations of the Total Number of H-Bonds Are Also Reported in the Second Row of Each Cell)

	IMI·DNA 1	IMI·DNA 2	ANT·DNA	ANT-DNA	DNA	IMI	ANT
drug	3	2	3	4		6	9
	3.6 ± 1.0	2.2 ± 0.8	4.3 ± 1.1	3.6 ± 0.9		2.3 ± 1.1	5.4 ± 1.3
DNA	9	8	13	8	14		
	8.6 ± 1.5	7.5 ± 1.4	8.8 ± 1.7	5.6 ± 1.1	11.4 ± 1.6		

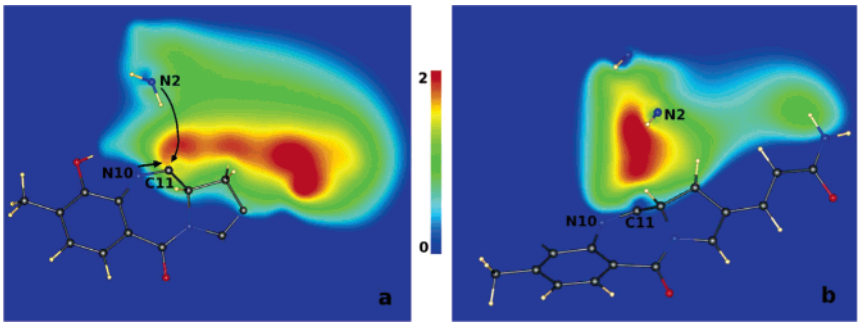

Figure 8. Contour plots of the electrostatic potential (volts) within the QM region, through the plane defined by atoms N2, N10, and C11. The plots report the difference in the electrostatic potential calculated *with* and *without bioframe*. Note that only in **IMI·DNA** (a) the largest difference is *localized* near the electrophilic carbon, while in **ANT·DNA** (b) it is *spread* in front of the reactive amino group of the guanosine. The N10−C11 arrow indicates the polarization of the bond, while the arrow between N2 and C11 indicates the gradient in ΔV.

electronic charge toward A (B) (see Methods). Such an analysis can be extended also to investigate the polarization of electron lone pairs of a given atom. In this case, the BI is defined in such a way that the larger the index, the stronger are the polarization effects on the lone pair. Here, we investigate the changes in BIs, averaged along the QM/MM trajectory, due to the inclusion of the electric field of the biomolecular frame. It is worth noticing that also little differences between these values are significant, because of the restricted range of values of the BO projection onto the bonds.[56] The N10−*C*11 π bond is the most polarized by the external electric field in **IMI·DNA 1** (where the drug is located in front of the reactive guanine) (note that, due to the delocalization of π bonds,[56] these results should be taken as an indication), while in **ANT·DNA** the largest effect is seen on the $N2_{G10}$ lone pair (Table S.6). Consistently, a large field is localized on the C11 atom in the first system (Figure 8). Thus, in **IMI·DNA 1**, the C11 atom is electron poorer than in vacuo, suggesting that DNA renders the complex more reactive. These results agree with experiments, which have shown a marked preference of anthramycin to bind double-stranded DNA (dsDNA), rather than single nucleobases.[1,3,65]

Concluding Remarks

While a large number of nanosecond-scale simulations of noncovalent drug/DNA complexes have appeared in the literature (see, e.g., refs 66−70), very few MD studies have been reported on alkylating drug/DNA systems, despite their pharmacological relevance.[71−73] Here, we have investigated by molecular mechanics simulations the noncovalent interaction between two forms of anthramycin present in solution (hydroxy and anhydro) and the 12-mer $d[GCCAACGTTGGC]_2$.

Our MD simulations suggest that the formation of the covalent complex does not affect the DNA helical axis, in agreement with experiments.[1] However, local structural changes are evident in both the DNA and the drug, consistent with the "induced fit mechanism" of binding proposed by Kizu et al.[9]

The noncovalent complexes are mainly stabilized by non-specific hydrophobic interactions, consistent with the modest sequence selectivity shown by these drugs.[5,6,14,74] In this respect, it is worth noting the remarkable difference observed in dynamical properties of the two forms of the drug. Hydroxy-anthramycin remains in the same site during the whole length of our simulation. In contrast, anhydro-anthramycin moves after ∼10 ns toward an adjacent site, and the system keeps the new configuration for the rest of the dynamics. Note that similar shuffling of minor groove binders has already been detected experimentally.[57] To the best of our knowledge, however, this is the first time that such a behavior is observed for minor groove alkylating drugs in a MD simulation. The sliding of the anhydro form is associated with an energetic and structural relaxation of the noncovalent complex, and is seen in a variety of additional simulations of the complex. The DNA conformation of the reactive complexes (i.e., with the drugs in front of its target guanine) is distorted relative to that assumed in solution or in the covalent complex. In particular, significant changes are observed in sugar, backbone, and helical parameters at the central region of the oligonucleotide. These values are associated with conformations higher in energy than that of canonical B-DNA. Interestingly, after the sliding of anhydro-anthramycin (nonreactive complex), the above structural parameters become similar to those of the free DNA. We conclude therefore that the oligonucleotide in the reactive complex is more distorted than in solution, in the observed nonreactive complex, and in the final product of the reaction. This requirement of a sizable structural distortion of the DNA frame and, to a lesser extent, of the drug could play a role in the experimentally observed

slower reactivity of anthramycin relative to that of other alkylating agents.[3]

Our MD simulations are complemented by QM/MM calculations. These show that the dsDNA electric field polarizes the reactive carbon of anhydro-anthramycin so as to render it more electrophilic. On the contrary, in the complex with hydroxy-anthramycin, the DNA field is unable to increase either the drug electrophilicity or the guanine nucleophilicity (although it clearly affects the electronic structure of the reactants). The field due to the water solvent appears instead to play a negligible role in both complexes. Thus, although the exact role of the electrostatic field of the environment can be established only if one simulates the entire alkylation reaction, our results suggest that the DNA frame assists the alkylation reaction by polarizing one of the reactants, at least in the case of the complex with anhydro-anthramycin. This is consistent with the experimental observation that the drug is able to covalently bind G-containing oligonucleotides but not guanine in aqueous solution.[1,3,65]

Acknowledgment. The authors thank Katrin Spiegel for her precious help. We are also grateful to Stefano Piana and Simone Raugei for useful suggestions. We are indebted to Prof. D. L. Beveridge for the critical reading of the manuscript. Computational resources have been granted by CINECA (INFM grants) and CASPUR. This project represents a scientific collaboration between the Trieste and Cagliari units of the INFM-Democritos. This work was supported in part by MIUR through project PON-CyberSar.

Supporting Information Available: Tables showing the box dimensions, number of waters, number of counterions, and simulated time for the various systems, force field parameters, RESP charges, hydrogen-acceptor distances and lifetimes, average values of minor groove widths, and bond ionicities and figures showing electrostatic forces and a comparison of rmsf's. This material is available free of charge via the Internet at http://pubs.acs.org.

References and Notes

(1) Kopka, M. L.; Goodsell, D. S.; Bailakov, I.; Grzeskowiak, K.; Cascio, D.; Dickerson, R. E. *Biochemistry* **1994**, *33*, 13593−13610.
(2) Hurley, L. H.; Chandler, C.; Garner, T. F.; Petrusek, R.; Zimmer, S. G. *J. Biol. Chem.* **1979**, *254*, 605−608.
(3) Hurley, L. H. *J. Antibiot.* **1977**, *30*, 349−370.
(4) Petrusek, R. L.; Uhlenhopp, E. L.; Duteau, N.; Hurley, L. H. *J. Biol. Chem.* **1982**, *257*, 6207−6216.
(5) Hertzberg, R. P.; Hecht, S. M.; Reynolds, V. L.; Molineux, I. J.; Hurley, L. H. *Biochemistry* **1986**, *25*, 1249−1258.
(6) Hurley, L. H.; Reck, T.; Thurston, D.; Langley, D. *Chem. Res. Toxicol.* **1988**, *1*, 258−268.
(7) Warpehoski, M. A.; Hurley, L. H. *Chem. Res. Toxicol.* **1988**, *1*, 315−333.
(8) Neidle, S. *Biopolymers* **1997**, *44*, 105−121.
(9) Kizu, R.; Draves, P. H.; Hurley, L. H. *Biochemistry* **1993**, *32*, 8712−8722.
(10) Remers, W. A.; Mabilia, M.; Hopfinger, A. J. *J. Med. Chem.* **1986**, *29*, 2492−2503.
(11) Alley, M. C.; Hollingshead, M. G.; Pacula-Cox, C. M.; Waud, W. R.; Hartley, J. A.; Howard, P. W.; Gregson, S. J.; Thurston, D. E.; Sausville, E. A. *Cancer Res.* **2004**, *64*, 6700−6706.
(12) Martin, C.; Ellis, T.; McGurk, C. J.; Jenkins, T. C.; Hartley, J. A.; Waring, M. J.; Thurston, D. E. *Biochemistry* **2005**, *44*, 4135−4147.
(13) James, A. M.; Blaikie, F. H.; Smith, R. A. J.; Lightowlers, R. N.; Smith, P. M.; Murphy, M. P. *Eur. J. Biochem.* **2003**, *270*, 2827−2836.
(14) Baraldi, P. G.; Bovero, A.; Fruttarolo, F.; Preti, D.; Tabrizi, M.; Pavani, M. G.; Romagnoli, R. *Med. Res. Rev.* **2004**, *24*, 475−528.
(15) Cornell, W. D.; Cieplak, P.; Bayly, C. I.; Gould, I. R.; Merz, K. M. J.; Ferguson, D. M.; Spellmeyer, D. C.; Fox, T.; Caldwell, J. W.; Kollman, P. A. *J. Am. Chem. Soc.* **1995**, *117*, 5179−5197.
(16) Cheatham, T. E., III; Cieplak, P.; Kollman, P. A. *J. Biomol. Struct. Dyn.* **1999**, *16*, 845−862.
(17) Wang, J.; Cieplak, P.; Kollmann, P. A. *J. Comput. Chem.* **2000**, *21*, 1049−1074.
(18) Darden, T.; York, D.; Pedersen, L. *J. Chem. Phys.* **1993**, *98*, 10089−10092.
(19) Beveridge, D. L.; McConnell, K. J. *Curr. Opin. Struct. Biol.* **2000**, *10*, 182−196.
(20) Cheatham, T. E., III; Young, M. A. *Biopolymers* **2001**, *56*, 232−256.
(21) Ponomarev, S. Y.; Thayer, K. M.; Beveridge, D. L. *Proc. Natl. Acad. Sci. U.S.A.* **2004**, *101*, 14771−14775.
(22) Jha, S.; Coveney, P. V.; Laughton, C. A. *J. Comput. Chem.* **2005**, *26*, 1617−1627.
(23) Cheatham, T. E., III. *Curr. Opin. Struct. Biol.* **2004**, *14*, 360−367.
(24) Rao, S. N.; Singh, U. C.; Kollman, P. A. *J. Med. Chem.* **1986**, *29*, 2484−2492.
(25) Zakrewska, K.; Pullman, B. *J. Biomol. Struct. Dyn.* **1986**, *4*, 127−136.
(26) Adams, L. J.; Jenkins, T. C.; Banting, L.; Thurston, D. E. *Pharm. Pharmacol. Commun.* **1999**, *5*, 555−560.
(27) Giudice, E.; Lavery, R. *Acc. Chem. Res.* **2002**, *5*, 350−357.
(28) Orozco, M.; Perez, A. N.; Luque, F. J. *Chem. Soc. Rev.* **2003**, *32*, 350−364.
(29) Freccero, M.; Gandolfi, R.; Sarzi-Amadé, M.; Rastelli, A. *J. Org. Chem.* **2005**, *70*, 9573−9583.
(30) Laio, A.; VandeVondele, J.; Rothlisberger, U. *J. Chem. Phys.* **2002**, *116*, 6941−6948.
(31) Becke, A. D. *Phys. Rev. A* **1988**, *38*, 3098−3100.
(32) Lee, C.; Yang, W.; Parr, R. G. *Phys. Rev. B* **1988**, *37*, 785−789.
(33) Frisch, M. J.; Trucks, G. W.; Schlegel, H. B.; Scuseria, G. E.; Robb, M. A.; Cheeseman, J. R.; Zakrzewski, V. G.; Montgomery, J. A., Jr.; Stratmann, R. E.; Burant, J. C. *Gaussian 98*, revision A.3; Gaussian, Inc.: Pittsburgh, PA, 1998.
(34) Pearlman, D. A.; Case, D. A.; Caldwell, J. W.; Ross, W. R.; Cheatham, T. E., III; DeBolt, S.; Ferguson, D.; Seibel, G.; Kollman, P. *Comput. Phys. Commun.* **1995**, *91*, 1−41.
(35) Jorgensen, W. L.; Chandrasekhar, J.; Madura, J. D.; Klein, M. L. *J. Chem. Phys.* **1983**, *79*, 926−935.
(36) Aaqvist, J. *J. Phys. Chem.* **1990**, *94*, 8021−8024.
(37) Wang, J.; Wolf, R. M.; Caldwell, J. W.; Kollman, P. A. *J. Comput. Chem.* **2004**, *25*, 1157−1174.
(38) Bayly, C. I.; Cieplak, P.; Cornell, W. D.; Kollman, P. A. *J. Phys. Chem.* **1993**, *97*, 10269−10280.
(39) Nosé, S. *Mol. Phys.* **1984**, *52*, 255−268.
(40) Hoover, W. G. *Phys. Rev. A* **1985**, *31*, 1695−1697.
(41) Parrinello, M.; Rahman, A. *J. Appl. Phys.* **1981**, *52*, 7182−7190.
(42) Hess, B.; Bekker, H.; Berendsen, H. J. C.; Fraaije, J. G. E. M. *J. Comput. Chem.* **1997**, *18*, 1463−1472.
(43) Varnai, P.; Djuranovic, D.; Lavery, R.; Hartmann, B. *Nucleic Acids Res.* **2002**, *30*, 5398−5406.
(44) Beveridge, D. L.; et al. *Biophys. J.* **2004**, *87*, 3799−3813.
(45) Berendsen, H. J. C.; van der Spoel, D.; van Drunen, R. *Comput. Phys. Commun.* **1995**, *91*, 43−56.
(46) Lindahl, E.; Hess, B.; van der Spoel, D. *J. Mol. Model.* **2001**, *7*, 306−317.
(47) Swaminatha, S.; Ravishanker, G.; Beveridge, D. L.; Lavery, R.; Etchebest, C.; Sklenar, H. *J. Mol. Model.* **1990**, *8*, 179−193.
(48) Lee, B.; Richards, F. *J. Mol. Biol.* **1971**, *55*, 379−400.
(49) Hutter, J.; Alavi, A.; Deutsch, T.; Ballone, P.; Bernasconi, M.; Focher, P.; Goedecker, S.; Tuckerman, M.; Parrinello, M. "CPMD", Max-Planck-Institut für Festkörperforschung, Stuttgart and IBM Research Laboratory Zürich, 1995−1999.
(50) Hohenberg, P.; Kohn, W. *Phys. Rev.* **1964**, *136*, B864−B871.
(51) Kohn, W.; Sham, L. J. *Phys. Rev.* **1965**, *140*, A1133−A1138.
(52) Sebastiani, D.; Rothlisberger, U. Advances in Density-functional-based Modeling Techniques—Recent Extensions of the Car-Parrinello Approach. In *Quantum Medicinal Chemistry*; Carloni, P., Alber, F., Eds.; Wiley-VCH: Weinheim, Germany, 2003; pp 5−36.
(53) Martyna, G. J.; Tuckerman, M. E. *J. Chem. Phys.* **1999**, *110*, 2810−2821.
(54) Troullier, N.; Martins, J. L. *Phys. Rev. B* **1991**, *43*, 1943−2006.
(55) Marzari, N.; Vanderbilt, D. *Phys. Rev. B* **1997**, *56*, 12847−12865.
(56) Alber, F.; Folkers, G.; Carloni, P. *J. Phys. Chem. B* **1999**, *103*, 6121−6126.
(57) Bailly, C.; Graves, D. E.; Ridge, G.; Waring, M. J. *Biochemistry* **1994**, *33*, 8736−8745.
(58) Gunz, D.; Naegeli, H. *Biochem. Pharmacol.* **1996**, *52*, 447−453.
(59) Hartmann, B.; Piazzola, D.; Lavery, R. *Nucleic Acids Res.* **1993**, *21*, 561−568.
(60) Wellenzohn, B.; Flader, W.; Winger, R. H.; Hallbrucker, A.; Mayer, E.; Liedl, K. R. *Biophys. J.* **2001**, *81*, 1588−1599.
(61) Wellenzohn, B.; Flader, W.; Winger, R. H.; Hallbrucker, A.; Mayer, E.; Liedl, K. R. *J. Am. Chem. Soc.* **2001**, *123*, 5044−5049.
(62) Schlitter, J. *Chem. Phys. Lett.* **1993**, *256*, 617−622.

(63) Teijeiro, C.; de la Red, E.; Marin, D. *Electroanalysis* **2000**, *12*, 963−968.
(64) Barkley, M. D.; Cheatham, S.; Thurston, D. E.; Hurley, L. H. *Biochemistry* **1986**, *25*, 3021−3031.
(65) Farmer, J. D., Jr.; Gustafson, G. R.; Conti, A.; Zimmt, M. B.; Suggs, J. W. *Nucleic Acids Res.* **1991**, *19*, 899−903.
(66) Harris, S. A.; Gavathiotis, E.; Searle, M. S.; Orozco, M.; Laughton, C. A. *J. Am. Chem. Soc.* **2001**, *123*, 12658−12663.
(67) Spackova, N.; Cheatham, T. E., III; Ryjacek, F.; Lankas, F.; van Meervelt, L.; Hobza, P.; Sponer, J. *J. Am. Chem. Soc.* **2003**, *125*, 1759−1769.
(68) Tanious, F. A.; Hamelberg, D.; Bailly, C.; Czarny, A.; Boykin, D. W.; Wilson, W. D. *J. Am. Chem. Soc.* **2004**, *126*, 143−153.
(69) Trieb, M.; Rauch, C.; Wellenzohn, B.; Wibowo, F. R.; Loerting, T.; Mayer, E.; Liedl, K. R. *J. Biomol. Struct. Dyn.* **2004**, *21*, 713−724.
(70) Dolenc, J.; Oostenbrink, C.; Koller, J.; van Gunsteren, W. F. *Nucleic Acids Res.* **2005**, *33*, 725−733.
(71) Romero, R. M.; Rojsitthisak, P.; Haworth, I. S. *Arch. Biochem. Biophys.* **2001**, *386*, 143−153.
(72) Spiegel, K.; Rothlisberger, U.; Carloni, P. *J. Phys. Chem. B* **2004**, *108*, 2699−2707.
(73) Ding, S.; Shapiro, R.; Geacintov, N. E.; Broyde, S. *Biochemistry* **2005**, *44*, 14565−14576.
(74) Denny, W. A. *Curr. Med. Chem.* **2001**, *8*, 533−544.
(75) Humphrey, W.; Dalke, A.; Schulten, K. *J. Mol. Graphics* **1996**, *14*, 33−38.
(76) Laaksonen, L. *J. Mol. Graphics* **1992**, *10*, 33−34.
(77) Bergman, D. L.; Laaksonen, L.; Laaksonen, A. *J. Mol. Graphics Modell.* **1997**, *15*, 301−306.